PAPER

CrossMark
click for updates

Activation of [CrCl$_3$\{PPh$_2$N(^{i}Pr)PPh$_2$\}] for the selective oligomerisation of ethene: a Cr K-edge XAFS study†‡

Stuart A. Bartlett,[ab] Jerome Moulin,[c] Moniek Tromp,[d] Gillian Reid,[c] Andy J. Dent,[e] Giannantonio Cibin,[e] David S. McGuinness[f] and John Evans*[ace]

The activation of the ethene tetramerisation catalyst system based upon [CrCl$_3$(THF)$_3$] and N(^{i}Pr)(PPh$_2$)$_2$ has been investigated *in situ* via the reaction of [CrCl$_3$\{PPh$_2$N(R)PPh$_2$\}(THF)] **1a** (R = ^{i}Pr) with excess AlMe$_3$ in toluene. The Cr K-edge XAFS spectrum of the solution freeze quenched after 1 min reaction time indicated monomethylation of the metal with the resultant product being [CrClMe(ClAlCl$_3$)\{PPh$_2$N(R)PPh$_2$\}(THF)] **4a** (R = ^{i}Pr). After 5 minutes reaction time the XAFS spectra indicate that ~50% of **4a** had been converted to a Cr(II) species, with the central core being high spin [CrCl$_2$\{PPh$_2$N(R)PPh$_2$\}] **7a** (R = ^{i}Pr); a similar species, [CrClMe\{PPh$_2$N(R)PPh$_2$\}] **9a** (R = ^{i}Pr) was observed as its adduct with AlMe$_3$ (**10a**) (R = ^{i}Pr) when spectra were recorded on samples maintained at room temperature. Detailed analysis (EXAFS and XANES) indicated that **7a** and **9a** are stabilised by adduct formation of a Cr–Cl bond to the Lewis acids B(C$_6$F$_5$)$_3$ and AlMe$_3$, respectively. Modelling with DFT methods indicated that five-coordination was achieved, respectively by Cr–F (**11a**) and Cr–C (**10a**) interactions. In the presence of [Ph$_3$C][Al\{OC(^{t}Bu^F)$_3$\}$_4$], the Cr XAFS of the room temperature solution was inconsistent with the maintenance of a phosphine complex, but could be modelled with a site like [Cr$_2$Me$_8$]$^{4-}$ \{Cr–Cr 2.01(2), Cr–C 2.14(4)\}, thus demonstrating considerable variation in the effects of differing Lewis acids.

^{a} *Research Complex at Harwell, Rutherford Appleton Laboratory, Didcot, OX11 0FA, UK. E-mail: stuart.bartlett@rc-harwell.ac.uk*

^{b} *Department of Chemistry, University of Bath, Bath, BA2 7AY, UK*

^{c} *Chemistry, University of Southampton, Southampton, SO17 1BJ, UK. E-mail: je@soton.ac.uk*

^{d} *Van't Hoff Institute for Molecular Sciences, University of Amsterdam, PO Box 94720, 1090 GS Amsterdam, Netherlands. E-mail: M.Tromp@uva.nl*

^{e} *Diamond Light Source, Rutherford Appleton Laboratory, Didcot, OX11 0DE, UK. E-mail: john.evans@diamond.ac.uk*

^{f} *School of Physical Sciences – Chemistry, University of Tasmania, Hobart 7001, Australia*

† Electronic supplementary information (ESI) available. See DOI: 10.1039/c6cy00902f
‡ Additional data available: XAFS spectra, XANES simulations and DFT calculations for all complexes are available to download from http://www.eprints.soton.ac.uk *via* doi: 10.5258/SOTON/395279.

1. Introduction

Ethene oligomerisation is an attractive method to produce linear alpha-olefins (LAOs), which are further used in the production of synthetic polymers, detergents, plasticisers and lubricants.[1] Employing metal catalysed oligomerisation of ethene can have a major drawback in the production LAOs, suffering from a statistical distribution of oligomer chain lengths.[2] Selective oligomerisation is possible due to major breakthroughs using homogeneous chromium catalysts to produce 1-hexene and/or 1-octene.[3,4] Using chromium with a bidentate diphenylphosphinoamine (PNP) in the presence of modified methylaluminoxane (MMAO) was seen to give 1-octene selectivity >70%.[5]

Evidence suggests this occurs *via* a metallacycle ring after oxidative coupling of ethene to chromium, followed by further insertion of ethylene at the Cr–C bond and finally, reductive elimination of 1-octene.[6,7] Despite this, the structure and oxidation state of the chromium intermediates are still not clear, with some studies favouring a Cr(II)/Cr(IV) synergy,[8,9] and others suggesting a Cr(I)/Cr(III) cycle[10–12] as the active pathway. One study has suggested a Cr-dimer, stabilised by PNP bridges.[13]

One previous study has used EPR and XAFS spectroscopy to help discriminate the active Cr species from Cr(acac)$_3$ and PPh$_2$N(^{i}Pr)PPh$_2$ in the presence of MMAO, in which the authors proposed the active chromium species to be [Cr^{II}(Me)$_2$(PPh$_2$N(^{i}Pr)PPh$_2$)].[14] However, in this investigation the XAFS measurements were acquired at 30 minutes per spectrum, with 5–10 scans averaged to achieve a good signal-to-noise, thus limiting the time resolution to hours. Herein we report mixing of [CrCl$_3$\{PPh$_2$N(R)PPh$_2$\}(THF)] **1a** (R = ^{i}Pr) with excess AlMe$_3$ in toluene, swiftly followed by freeze-quenching and subsequent analysis by XAFS spectroscopy. The reaction was frozen at predetermined intervals down to 1 minute from mixing, using a technique used in previous

experiments.[15–18] The analysis of these reactions by XAFS spectroscopy also enabled a more thorough analysis of data previously collected from the same reaction during tens of minutes at room temperature, without freeze-quenching.[19] The present analysis is aided by density functional theory (DFT) calculations, with a survey performed on [CrCl$_3$\{PPh$_2$N(R)PPh$_2$\}(THF)] **1b** (R = Me).

This analysis sheds new light on of the role of the aluminium and other co-catalysts during ethene tetramerisation, investigating the promotional effects previously reported.[20] Here we present the first instance of conclusive structural data at much shorter time scales (1 and 5 minutes) for the species trapped in the solution phase, formed by the reaction of this highly valuable tetramerisation catalyst and its aluminum activator. This contrasts with previous studies that have allowed the reaction to proceed during analysis or have been crystallised out of solution over long time scales.

2. Results and discussion

2.1 Structure of complex 1

The Cr K-edge XANES and EXAFS data of complex **1a** are presented in Fig. 1. The EXAFS analysis is consistent with the 6-fold coordination, with Cr–O, Cr–Cl and Cr–P shells at 2.05, 2.28(1) and 2.48(2) Å, respectively; the N atom in the chelate ring was also modelled in the fit presented (Fig. S1 and Tables 1 and S1†). Due to its low solubility in toluene, solution phase structural data for **1a** were difficult to obtain and so the powder data have been used as a structural comparison.

A set of DFT models was compared in terms of predicting the Cr–E distances of complexes close to those in this study.
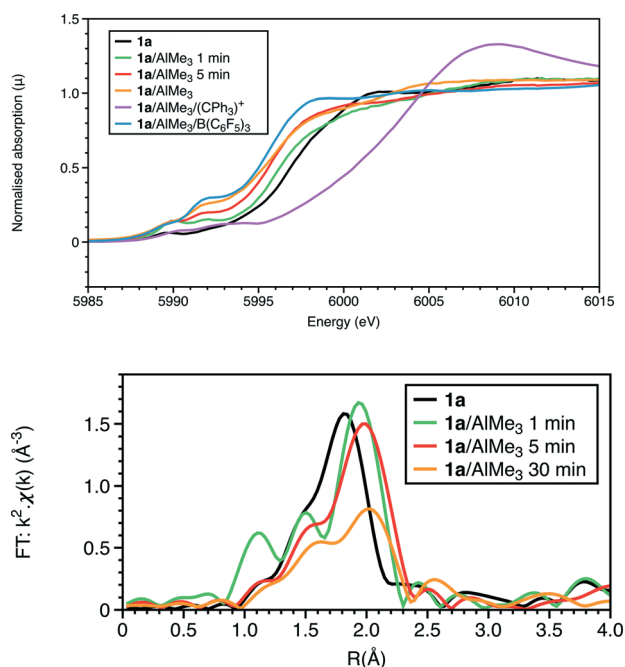

Fig. 1 At the Cr K-edge: (top) XANES and (bottom) Fourier transforms of k^2-weighted EXAFS data. Reactions performed at ambient temperature, some quenched by liquid nitrogen after a set reaction time.

Table 1 Structural parameters from Cr K-edge EXAFS analysis for **1a** in BN (boron nitride), 5 mM in toluene when reacting with excess AlMe$_3$. Reactions performed at ambient temperature, some quenched by liquid nitrogen after a set reaction time

Cr reaction	Coordination shell	d(Cr–X) (Å)
1a in BN	1Cr–O	2.05[a]
	3Cr–Cl	2.28(1)
	2Cr–P	2.48(2)
	1Cr⋯N	2.96(8)
Quenched after 1 minute	2Cr–C/O	2.03(4)
	2Cr–Cl	2.37(1)
	2Cr–P	2.54(6)
Quenched after 5 minutes	1Cr–C	2.10(1)
	2Cr–Cl	2.37(3)
	2Cr–P	2.49(2)
Ambient temperature after 30 minutes	1Cr–C	2.14(2)
	2Cr–P	2.49(1)
Ambient temperature, with B(C$_6$F$_5$)$_3$	1Cr–Cl	2.73(3)
	2Cr–Cl[a]	2.36(2)
	2Cr–P[a]	2.472(8)
	1Cr–C[a]	3.04(1)
Ambient temperature, [Ph$_3$C][Al\{OC(^{t}Bu^F)$_3$\}$_4$]	1Cr–Cr[a]	2.01(2)
	3.3(7)Cr–C	2.14(4)

[a] Fixed parameters.

Quartet states were adopted for Cr(III) species, and quintet states were established to be the most stable spin states for the Cr(II) complexes. Accordingly, [CrCl$_3$\{PPh$_2$N(Cy)PPh$_2$\}(NCMe)] (Cy = cyclohexyl)[21] was chosen as a base structure due to its similarity to complex **1a** (R = ^{i}Pr), albeit a *fac* rather than a *mer* isomer. The tendency for all methods was for an overestimate of the bond length compared to those determined in the crystal structure of this complex (Table S2†), but this difference was less for EDF2 and ωB97X-D functionals compared to the results using B3LYP. The EDF2/6-31G* method was employed in a wide survey of reaction possibilities starting from the reagents CrCl$_3$(THF)$_3$, PPh$_2$N(Me)PPh$_2$ and Al$_2$Me$_6$, and the more likely species probed by several DFT methods for R = Me and ^{i}Pr. This showed that the *mer* isomers of both the *tris* THF complex and complex **1b** were more stable than the *fac* ones (structures in Fig. 2 and $\Delta G°$ in Fig. 3).
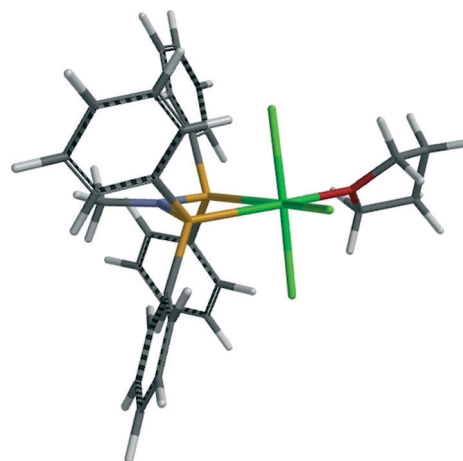
1b

(Yellow = Cr, green = Cl, red = O, brown = P, grey = C, purple = N and white = H).

A comparison of the EXAFS results for complex **1a** and DFT models (Table 2) shows that the observed and calculated Cr–O and mean Cr–Cl distances are within 0.03 Å of each other. The *fac* isomer **2b** displays a much longer Cr–O distance (2.18 Å) than observed experimentally, giving further support for the assignment of the *mer* isomer **1**. The observed Cr–P bond length is similar to those previously reported *fac*-[CrCl₃{PPh₂N(Cy)PPh₂}(NCMe)].[21] The calculated structures display significant interdependent *trans* effects. There is a lengthening of the other Cr–P distance to 2.60 Å and a shortening of the Cr–Cl distance *trans* to it (2.27 Å); these distortions were not distinguishable from the EXAFS data.

2.2 Reaction of complex 1 with excess AlMe₃

The UV-visible spectrum of **1a** displays two d–d transitions with maxima at 701 and 502 nm, which may be anticipated as arising from a $^4A_2$ ground state to $^4T_2$ and $^4T_1(F)$ excited
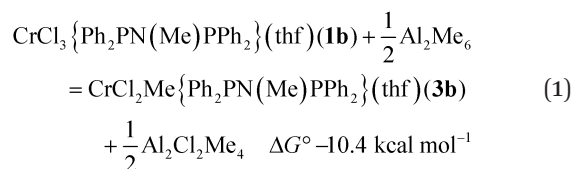
states (Fig. S2†). TDDF calculations based upon the refined structure of **1a** afforded clusters of peaks in the range of 620–720 and 450–550 nm (Fig. S3†). As we have reported for other ligand systems,[17,22] the addition of AlMe₃ to a solution of **1a** in toluene at ambient temperature with spectra recorded within 2–3 minutes of the addition, results in a shift of the first absorption peak to shorter wavelength (660 nm) with a possible shoulder (∼450 nm) on the tail of an intense, charge-transfer band in the UV (Fig. S2†).

2.3 Freeze-quench XAFS of the reaction of complex 1 with AlMe₃ after 1 minute

Complex **1a** is sparingly soluble in toluene, and decomposes to the dimer [CrCl₃{PPh₂N(ⁱPr)PPh₂}]₂.[5] This made the solution mixing by stopped flow methods from stock solutions, as employed previously in other chemical systems,[15–18] an unsuitable technique. Instead, to investigate the early stages of the activation process using freeze-quenched solutions, a solution of AlMe₃ in toluene was added to a suspension of **1a** in toluene in a Schlenk tube, mixed rapidly and transferred quickly to a Kapton tube and the sample frozen to 77 K using liquid nitrogen, measured at 1.0 minute and 5.0 minutes elapsed time from point of mixing.

The Cr K-edge XAFS spectra obtained from room temperature reaction of **1a** in toluene with a 20 fold excess AlMe₃ and frozen 1 minute after mixing {Fig. 1 (green)} show that a structural change is evident. EXAFS analysis (Fig. S5, Table S3†) is consistent with a substitution of 1 Cr–Cl ligand by a Cr–Me group. The combined Cr–O/C shell is refined to a similar distance to the Cr–C in **1a** (2.03 Å), but there is a lengthening of both the Cr–Cl and Cr–P distances to 2.37(1) and 2.54(6) Å, respectively. This would suggest the product to be [CrCl₂Me{PPh₂N(R)PPh₂}(THF)] (R = ⁱPr) **3a**.

There are 4 possible geometric isomers of the complex **3a**; DFT calculations on the reaction of **1b** with AlMe₃ (eqn (1)) indicate that the most stable is that shown for **3b** in Fig. 2, with *trans* chloride ligands, consistent with the substitution of a Cr–Cl in **1a** *trans* to a Cr–P bond. Direct substitution of a mutually *trans* chloride in **1a** provided an isomer calculated to be 6.2 kcal mol⁻¹ less stable, and the two isomers requiring rearrangement of the THF ligand to becoming *cis* to both P atoms of the phosphine ligand were found to be less stable still (7.7 and 9.3 kcal mol⁻¹).

Fig. 2 Structures considered for the reaction of [CrCl₃{PPh₂N(R)PPh₂}(THF)] **1** (a R = ⁱPr, b R = Me) with AlMe₃.

$$CrCl_3\{Ph_2PN(Me)PPh_2\}(thf)(\mathbf{1b}) + \frac{1}{2}Al_2Me_6$$
$$= CrCl_2Me\{Ph_2PN(Me)PPh_2\}(thf)(\mathbf{3b}) \qquad (1)$$
$$+ \frac{1}{2}Al_2Cl_2Me_4 \quad \Delta G° -10.4 \text{ kcal mol}^{-1}$$

Calculated bond lengths from DFT methods are presented in Table 3, with the EXAFS-derived distances obtained from the freeze-quenched solution after 1 minute. The combined C/O shell agrees very closely with the calculated Cr–C distance from the most stable isomer of **3b** (2.04 Å), and the
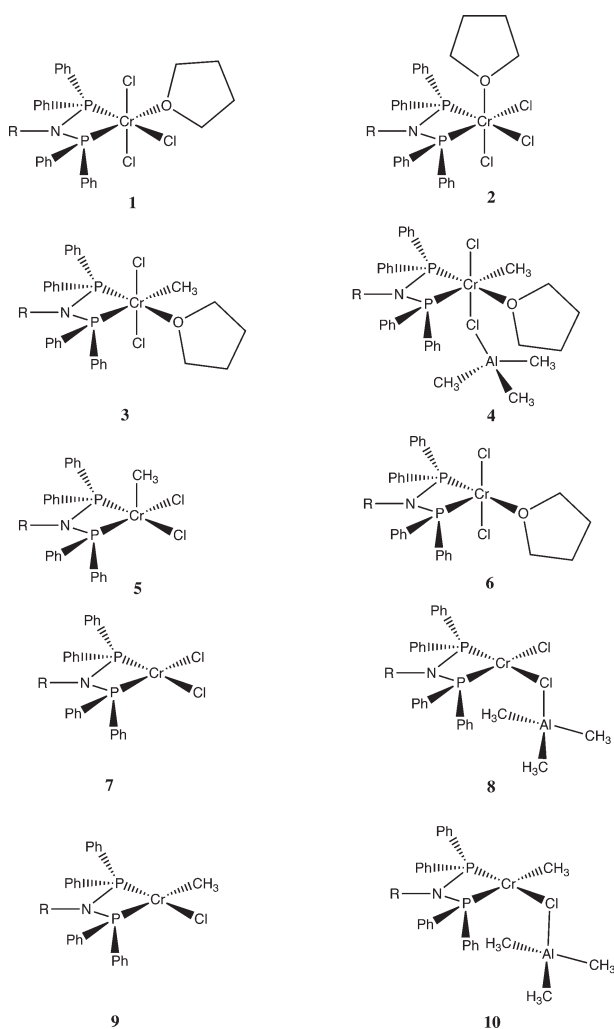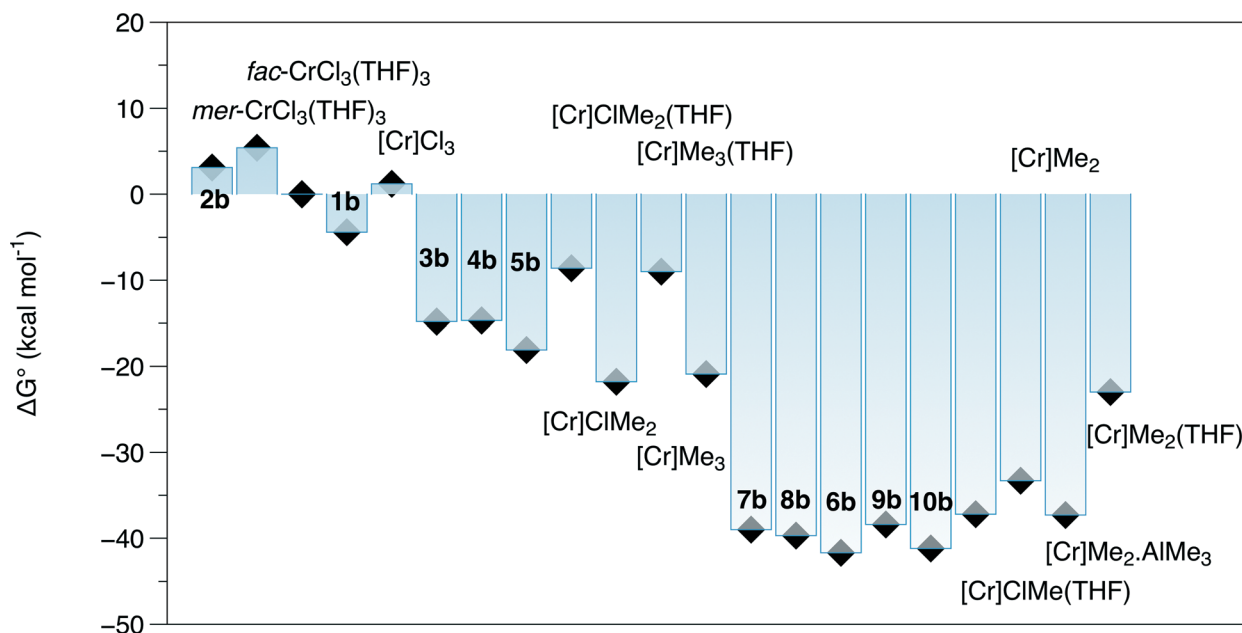
Fig. 3 ΔG° calculated by EDF2/6-31G* for reactions from CrCl$_3$(THF)$_3$, (PPh$_2$)$_2$NMe and Al$_2$Me$_6$. Compound numbers as in Fig. 2, [Cr] = Cr(PPh$_2$(NMe)PPh$_2$). Cr(III) and Cr(II) complexes S = 3/2 and S = 2, respectively.

Table 2 Comparison of the Cr–E bond lengths from the Cr K-edge EXAFS analysis of **1a** (R = ^{i}Pr) with results from density functional calculations

	Distances (Å)		
	1Cr–O	3Cr–Cl	2Cr–P
EXAFS: **1a**	2.05	2.28(1)	2.48(2)
1b: EDF2/6-31G*	2.064	2.274, 2.315, 2.331	2.461, 2.648
EDF2/6-31G**	2.065	2.277, 2.324, 2.326	2.469, 2.626
ωB97X-D/6-31G*	2.067	2.268, 2.303, 2.330	2.450, 2.634
ωB97X-D/6-31G**	2.066	2.268, 2.303, 2.333	2.454, 2.630
1a: EDF2/6-31G*	2.072	2.277, 2.318, 2.316	2.464, 2.647
EDF2/6-31G**	2.059	2.280, 2.324, 2.328	2.455, 2.638
ωB97X-D/6-31G*	2.070	2.273, 2.309, 2.333	2.452, 2.620
ωB97X-D/6-31G**	2.070	2.271, 2.312, 2.330	2.453, 2.617
2b: EDF2/6-31G*	2.178	2.283, 2.284, 2.286	2.550, 2.584
EDF2/6-31G**	2.174	2.283, 2.285, 2.286	2.551, 2.583
ωB97X-D/6-31G*	2.180	2.280, 2.282, 2.283	2.523, 2.567
ωB97X-D/6-31G**	2.178	2.281, 2.284, 2.284	2.524, 2.560

Table 3 Comparison of the Cr–E bond lengths from the Cr K-edge EXAFS analysis of **1a** (R = ^{i}Pr)/AlMe$_3$ quenched after 1 minute with those for **3a**, **3b** and adducts of **3b** with AlMe$_3$ from selected density functional calculations

	Distances (Å)		
	Cr–C/O	Cr–Cl	Cr–P
EXAFS: **4a**	2 at 2.04(5)	2 at 2.38(2)	2 at 2.54(6)
3a Cl *trans* Cl			
EDF2/6-31G*	2.048 (C)	2.333	2.503
	2.088 (O)	2.352	2.745
ωB97X-D/6-31G**	2.043 (C)	2.321	2.480
	2.095 (O)	2.361	2.703
3b Cl *trans* Cl			
EDF2/6-31G*	2.047 (C)	2.333	2.497
	2.081 (O)	2.337	2.816
ωB97X-D/6-31G**	2.034 (C)	2.317	2.484
	2.079 (O)	2.355	2.791
3a Me *trans* Cl			
EDF2/6-31G*	2.076 (C)	2.298	2.458
	2.087 (O)	2.411	2.669
ωB97X-D/6-31G**	2.071 (C)	2.296	2.441
	2.106 (O)	2.428	2.586
3b Me *trans* Cl			
EDF2/6-31G*	2.088 (C)	2.313	2.467
	2.089 (O)	2.414	2.552
ωB97X-D/6-31G**	2.076 (C)	2.308	2.453
	2.095 (O)	2.421	2.555
3b Cl *trans* Cl; with 1Cr–Cl–AlMe$_3$ (**4b**)			
EDF2/6-31G*	2.038 (C)	2.314	2.509
	2.076 (O)	2.402	2.822
3b Cl *trans* Cl; with 2Cr–Cl–AlMe$_3$			
EDF2/6-31G*	2.039 (C)	2.365	2.518
	2.057 (O)	2.377	2.799
3b Cl *trans* Cl; with 1Cr–C–AlMe$_3$			
EDF2/6-31G*	2.083 (C)	2.325	2.514
	2.073 (O)	2.334	2.727

Cr–O distance (2.08 Å) is within experimental error. Moving the methyl group to a position *trans* to Cr–Cl in the second most stable isomer increases the Cr–C distance to the region of 2.08 Å, towards the end of the extreme of the standard deviation of the EXAFS analysis. The mean of the calculated Cr–Cl distances (2.34 Å) is 0.04 Å less than the distance refined from the EXAFS by 2 standard deviations. Switching to the alternative isomer, with the Cr–Me *trans* to Cr–Cl, does increases that distance to Cl, as would be expected from the *trans*-influence of the alkyl group, but there is a compensating reduction in the other Cr–Cl bond length. An alternative way to increase the Cr–ligand bond lengths would be to form an adduct with AlMe$_3$, which was in large excess. The binding of 1 AlMe$_3$ to Cl, as in complex **4b** is essentially neutral in terms of free energy (ΔG° = 0.1 kcal mol^{-1}); the binding of a

second AlMe$_3$ to a Cr–Cl (ΔG° = 4.6 kcal mol^{-1}), and the binding to the Cr–Me group (ΔG° = 8.0 kcal mol^{-1}) are endoergic.

In addition to lengthening the mean Cr–Cl distance by ~0.02 Å, the effects of the AlMe$_3$ binding to a Cr–Cl unit are to reduce the Cr–O and Cr–C bond lengths, affording a mean distance for that combined shell of 2.05 Å, within experimental error of the refined value. As compared to complex **1**, the methyl group has a strong lengthening influence on the *trans* Cr–P bond, and thus making fitting the Cr–P shell potentially problematical due to the separation of the two distances by ~0.3 Å. An alternative fitting model was attempted splitting this shell (Fig. S6, Table S4†) which afforded Cr–P distances of 2.45(6) and 2.60(2) Å. This had little effect on the R factor of the fit, but the Debye–Waller factors for the split Cr–P shells came into line with that of the Cr–Cl shell. The free energy calculations on these reactions places (Fig. 3) the structures for [CrCl$_2$Me{PPh$_2$N(R)PPh$_2$}(THF)] (R = Me) **3b** and its AlMe$_3$ adduct **4b** as both being 11 kcal mol^{-1} more favourable that the initial reagents. Given the excess of the aluminium reagent, assignment of structure **4a** as the reaction product observed after 1 minute of reaction appears reasonable.

Given the challenges of establishing coordination numbers of minor shells, two alternatives with a lower coordination number for the Cr–O/C shell were considered: the Cr(III) complex **5a** and the Cr(II) species **6a**. The calculated Cr–Cl bond lengths (Table 4) of **5b** were significantly shorter than the experimental ones (by 0.12 Å), rendering it less probable option. The XANES for the two 5-coordinate species **5b** and **6b** were calculated in addition to the 6-coordinate complex **3b**
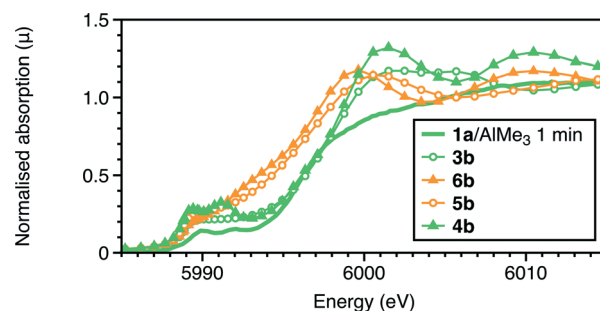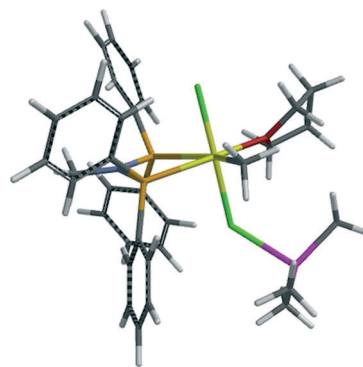

Fig. 4 Comparison of the experimental Cr K-edge XANES of the reaction quenched after 1 minute with those calculated for complexes **3b**, **4b**, **5b** and **6b**.

(Fig. 4). It is the 6-coordinate centres **3b** and **4b** which more closely match the experimental features as both the 5 coordinate complexes are predicted to display a much larger shift to low energy as compared to the precursor, **1a**. The model of **4b** also replicates the two pre-edge features more closely than **3b**, giving further support to this proposal.

The calculated UV-visible spectra of **3b** and **4b** (Fig. S3†) both show an increase in intensity of the band near 400 nm, and a shift of the lowest energy band to lower energy, consistent with the experimental observations; the adduct formation with AlMe$_3$ does reduce the magnitude of the shift. The calculated UV-visible spectrum of one of the most stable of the Cr(II) species, **8b**, is radically different from that observed a few minutes after mixing. This also provides evidence for the first-observed species remaining Cr(III), in contrast to our observations using the RS(CH$_2$CH$_2$)$_2$NH ligand system.[17]

Table 4 Comparison of the Cr–E bond lengths from the Cr K-edge EXAFS analysis of the 5 minute reaction of **1a** (R = ^{i}Pr) with AlMe$_3$ and recorded at ambient temperature (30 minute scans) with those calculated for **5** to **10** from selected density functional calculations

	Distances (Å)		
	Cr–C/O	Cr–Cl	Cr–P
EXAFS (after 5 minutes)	1 at 2.10(1)	2 at 2.37(3)	2 at 2.49(2)
EXAFS (after 30 minutes)	1 at 2.14(3)	1 at 2.73(3)	2 at 2.49(1)
EXAFS, with B(C$_6$F$_5$)$_3$, ambient	1 at 3.04(1)	2 at 2.36(2)	2 at 2.472(8)
5b: EDF2/6-31G*	2.036 (C)	2.258, 2.267	2.513, 2.544
ωB97X-D/6-31G**	2.034 (C)	2.268, 2.268	2.477, 2.498
6b: EDF2/6-31G*	2.089 (O)	2.339, 2.341	2.552, 2.768
ωB97X-D/6-31G**	2.089 (O)	2.340, 2.356	2.555, 2.711
7a: EDF2/6-31G*		2.281, 2.284	2.483, 2.486
ωB97X-D/6-31G**		2.284, 2.293	2.470, 2.483
7b: EDF2/6-31G*		2.280, 2.282	2.488, 2.510
ωB97X-D/6-31G**		2.286, 2.286	2.495, 2.500
8b: EDF2/6-31G*	2.850 (C)	2.283, 2.378	2.492, 2.524
ωB97X-D/6-31G**	2.584 (C)	2.286, 2.414	2.469, 2.533
9a: EDF2/6-31G*	2.067 (C)	2.289	2.445, 2.584
ωB97X-D/6-31G**	2.078 (C)	2.299	2.457, 2.566
9b: EDF2/6-31G*	2.064 (C)	2.289	2.467, 2.606
ωB97X-D/6-31G**	2.072 (C)	2.299	2.459, 2.596
10a: EDF2/6-31G*	2.067 (C), 2.881 (C)	2.396	2.456, 2.589
ωB97X-D/6-31G**	2.069 (C), 2.345 (C)	2.596	2.435, 2.556
10b: EDF2/6-31G*	2.067 (C), 2.862 (C)	2.390	2.466, 2.641
ωB97X-D/6-31G**	2.070 (C), 2.592 (C)	2.443	2.456, 2.589

4b

(Yellow = Cr, light green = Cl, red = O, brown = P, grey = C, purple = N, magenta = Al and white = H).

2.4 Freeze-quench XAFS of the reaction of complex 1 with AlMe$_3$ after 5 minutes

The Cr K-edge XANES and EXAFS spectra of a freeze-quenched sample show a further change when the reaction time was increased to 5 minutes. When repeating the reaction and freezing at 1 minute in the presence of a Lewis acid, [Ph$_3$C][Al{OC(^{t}Bu^F)$_3$}$_4$], identical spectra to that of the reaction frozen at 5 minutes, without [Ph$_3$C][Al{OC(^{t}Bu^F)$_3$}$_4$], were

observed. The main difference in the result of the EXAFS analysis (Fig. 1, S7 and S5, Tables 1, S5 and S3†) is the reduction of the coordination of the first shell from 2 to 1. This was modelled as 1Cr–C at 2.10(1) Å, but it may alternatively be due to an oxygen shell. Thus the possibilities for the coordination centre could include the 5 coordinate Cr^{III} centre like $[CrCl_2Me\{PPh_2N(R)PPh_2\}]$ (R = ^iPr) **5a** or a Cr^{II} site like $[CrCl_2\{PPh_2N(R)PPh_2\}(THF)]$ (R = ^iPr) **6a**. Alternatively, this spectrum could represent a mixture of the first observed species, **4a**, and the longer-lived product observable in room temperature samples. To test this, we performed linear combination fitting analysis (LCA) of the data from the reaction frozen after 5 minutes, starting by comparing 1:1 mixtures of the data collected at 1 minute reaction time with one of the ambient temperature reactions with and without $B(C_6F_5)_3$, given as $[CrCl_2\{PPh_2N(R)PPh_2\}]$ or $[CrClMe\{PPh_2N(R)PPh_2\}]$ complexes from the EXAFS analysis (Table 1), respectively. The LCA gave 3:2 mixture of product at 1 min and ambient temperature reaction without $B(C_6F_5)_3$ (R = 0.06%). A better LCA fit is achieved when using the ambient temperature reaction with $B(C_6F_5)_3$ as a standard, giving a 1:1 mixture with the product at 1 minute (R = 0.01%) (Fig. 5). The XANES features show a progressive shift of the main absorption edge to lower energy from that of **1a** through the two freeze quench measurements to the room temperature scans.

The free energy reaction survey (Fig. 3) indicated a very favourable reductive elimination reaction (2) to **7b** (in a high spin state, S = 2). This is similar to the results obtained for the activation of $[CrCl_3\{RS(CH_2CH_2)_2NH\}]$,[17] with the $\Delta G°$ gain in forming and eliminating ethane providing the driving force for the reaction. We note that reductive elimination from Cr^{III} alkyls has been previously reported,[23] but have no further evidence to distinguish possible mechanisms. The additions of either THF to **7b** to form **6b** or AlMe$_3$ (to **8b**) were slightly exoergic.

$$CrCl_2Me\{Ph_2PN(Me)PPh_2\}(\mathbf{5b})$$
$$= CrCl_2\{Ph_2PN(Me)PPh_2\}(\mathbf{7b}) \qquad (2)$$
$$+ \frac{1}{2}C_2H_6 \quad \Delta G° -20.9 \text{ kcal mol}^{-1}$$

The most stable species calculated (Fig. 3) were the 4-coordinate $Cr(II)$ species **7** and **9** and their adducts with THF and AlMe$_3$. However, $\Delta G°$ for eqn (3) (−7.1 kcal mol^{-1}) is more favourable than the binding of THF to the $Cr(II)$ centres. Hence, if released, THF should be sequestered on aluminium.

$$0.5 \ Al_2Me_6 + THF = AlMe_3(THF) \quad \Delta G° -7.1 \text{ kcal mol}^{-1} \quad (3)$$

The bond lengths calculated for these complexes (**5** to **8**), and $[CrClMe\{PPh_2N(R)PPh_2\}]$ **9**, and its adduct with AlMe$_3$ involving a bridging chloride **10** (Fig. 2), are presented in Table 4. There is no evidence that any unique species has been trapped after a reaction time of 5 minutes, rather that there is conversion from **4a** to the room temperature, steady state species.

2.5 XAFS of complex 1 with excess AlMe$_3$ at ambient temperature

2.5.1 Without additional Lewis acid. EPR studies on glasses frozen ~10 min after addition of AlMe$_3$ to a solution of **1a** showed loss of the signal from **1a** (Fig. S4†), and are consistent with a change in coordination sphere and/or oxidation state. The Cr K-edge XANES of the reaction solutions maintained at ambient temperature for up to 1 hour were similar in the presence or absence of the Lewis acid $B(C_6F_5)_3$ and displayed a further edge shift to lower energy (Fig. 1a). The EXAFS analysis of the spectrum acquired after 1 hour reaction time at room temperature afforded a primary coordination sphere of 2Cr–P and one Cr–C shell (Fig. S8, Tables 1 and S6†). There fit was improved by the incorporation of a long Cr–Cl distance (2.73(3) Å), as might be anticipated in structure **10**, an exoergic adduct of the $Cr(II)$ complex **9** and AlMe$_3$ (Fig. 3). The structures derived from the DFT calculations of **10** were very sensitive on the method and give rise to considerable uncertainty in the asymmetry of the Cr–Cl–Al–C ring.

2.5.2 Effect of $[Ph_3C][Al\{OC(^tBu^F)_3\}_4]$. The incorporation of a different Lewis acid, $[Ph_3C][Al\{OC(^tBu^F)_3\}_4]$, resulted in a marked change in the XANES pattern, with an edge shift to higher energy (Fig. 1a). Such observations are consistent with an increase in the degree of alkylation of the chromium centre.[14,17,24]

The EXAFS also shows a marked change with the addition of the trityl-containing Lewis acid (Fig. 6, 7 and S9; Tables 1
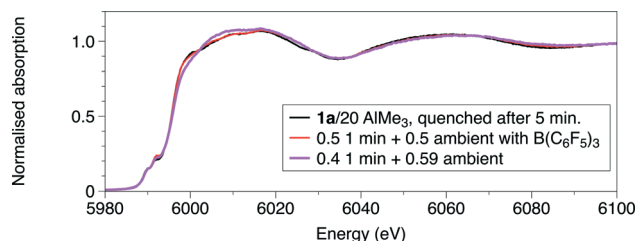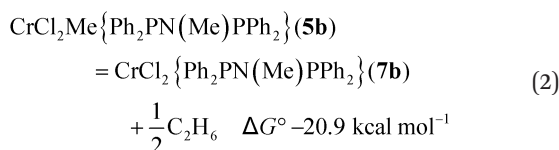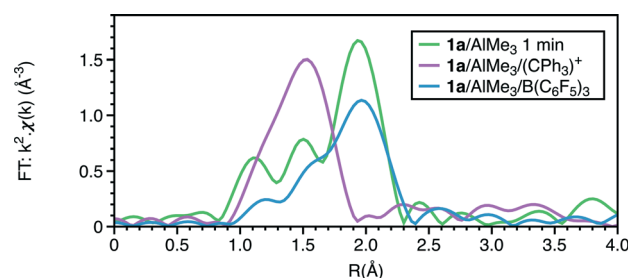

Fig. 5 Comparison of the experimental Cr K-edge XANES of the reaction quenched after 5 minutes with spectra of a combination of a 2:3 combination of the spectrum from a sample quenched after 1 minute, and of the room temperature measurement and a 1:1 combination of the spectrum from a sample quenched after 1 minute, and of the room temperature measurement with solution containing $B(C_6F_5)_3$.

Fig. 6 Cr K-edge Fourier transforms of k^2-weighted EXAFS data of reactions of **1a** with 20AlMe$_3$ (1 min); **1a** + 30AlMe$_3$ + 1[Ph$_3$C][Al{OC(^{t}Bu^F)$_3$}$_4$]; **1a** + 30AlMe$_3$ + 1B(C$_6$F$_5$)$_3$.
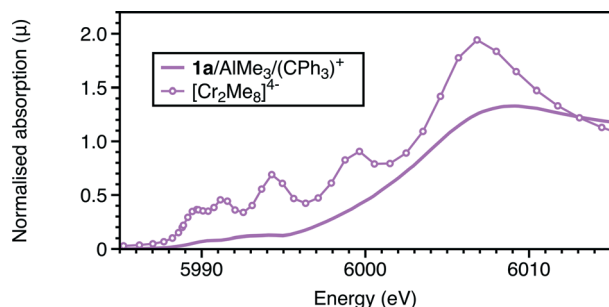
Fig. 7 Cr K-edge XANES: experimental and calculated spectra of **1a** with AlMe$_3$ with (CPh$_3$)[Al{OC(^{t}Bu^F)$_3$}$_4$].

and S7†). The results from this analysis suggest the initial chromium complex has undergone complete alkylation to lose the PNP ligand and form a short Cr–Cr multiple bond. The refined Cr–Cr bond length (2.01(2) Å) is close to that reported for the quadruple bond in the Cr(II) salt Li$_4$[Cr$_2$Me$_8$]] ·4THF,[25] and the calculated shift in the edge energy for Li$_4$[Cr$_2$Me$_8$]] also matches those of this reaction product. The EXAFS and XANES together do indicate that the effect of [Ph$_3$C][Al{OC(^{t}Bu^F)$_3$}$_4$] is the dissociation of the bidentate phosphine ligand and the formation of a highly alkylated Cr(II) metal–metal bonded dimer, but its complete formulation is uncertain. When freezing at 1 minute reaction time, we did not observe **4a** in the presence of [Ph$_3$C][Al{OC(^{t}Bu^F)$_3$}$_4$] suggesting that it quickens the change from **1a** to the phosphine-containing Cr(II) site prior to its dissociation.

2.5.3 Effect of [B(C$_6$F$_5$)$_3$]. The Cr K-edge EXAFS analysis the reaction of **1a** with 30 equiv. AlMe$_3$ and 1 equiv. [B(C$_6$F$_5$)$_3$] (Fig. 6, 8, S10 and S11; Tables 1 and S8†) indicate the maintenance of a chloro-phosphine complex, possibly also in a Cr(II) site, which is consistent with the $\Delta G°$ changes in Fig. 3. The EXAFS analysis indicated loss of the Cr–O/C coordination to form a four coordinate centre, such as that in **7** (Table 4). However, the calculated XANES for structure **7b** affords an edge position of relatively higher energy (Fig. S12†).

The calculated Cr–P distances for **7** are close to those provided by the EXAFS analysis, but the Cr–Cl shell is again shorter than the experimental value, by ~0.08 Å. The EXAFS analysis has provided significant evidence, albeit inconclusive, for a light atom shell near 3.0 Å because when including this shell, the R-factor is greatly reduced to give a better overall fit. Accordingly, the interactions of BR$_3$ (R = Me, Ph and C$_6$F$_5$) and AlMe$_3$ with **7** at Cl and Cr were modelled using EDF2 and ωB97X-D functionals. Using EDF2/6-31G**, interaction of BMe$_3$ to **7b** was found to be extremely weak and involving a long Cr···HB distance (3.467 Å). This distance was reduced in the BPh$_3$ adduct (3.135 Å), with an energy gain of 4.5 kcal mol^{-1}; this would not be sufficient to offset the entropy loss by complexation at room temperature. The binding of AlMe$_3$ to **7b**, forming **8b**, is stronger ($\Delta H°$ −8.6 kcal mol^{-1}), and complex formation is slightly exoergic (Fig. 3). The structural effects are to increase the Cr–Cl distance for the bridging chloride to 2.378 Å, close to the experimental value. Also,

one methyl group was calculated to bend back to take up an apical coordination site with a long Cr···C interaction (2.85 Å). This weaker interaction is strongly functional dependent. Using the ωB97X-D functional, which specifically includes long-range interactions[26] and has proven effective in calculating reaction energies,[27] the Cr–Cl(Al) is lengthened further (2.414 Å) and the Cr–C(Al) distance further reduced (2.58 Å). Inclusion of this interaction.

A different type of interaction to the metal is afforded by B(C$_6$F$_5$)$_3$. Binding of this Lewis acid to **7a** and **7b** was two-fold in nature: boron to chloride (~3.2 and 3.0 Å from EDF2 and ωB97X-D respectively), and a C–F group *ortho* to boron (Cr–F 2.55–2.65; Cr–C 3.19–3.35 Å) in complex **11** (a = ^{i}Pr; b = Me). The effect of this coordination on the Cr–Cl and Cr–P distances is to increase the former by ~0.1 Å and decrease the latter by ~0.2 Å. Formation of **11b** using EDF2/6-31G* was calculated to be exothermic (−13.2 kcal mol^{-1}), but endoergic (4.8 kcal mol^{-1}). However, using the alternative functional, which afforded the closer interactions of the C–F group to boron, rendered complexation more exothermic (−25 kcal mol^{-1}), and thus the adduct **11a** might be anticipated. Such interactions would be difficult to observe definitively by EXAFS from the Cr edge. There is though some evidence for a long light atom distance modelled as a Cr–C distance (3.04 Å). However, the calculated XANES for this aligns more closely to the experimental spectrum than that of complex **7a** (Fig. 8 and S12†). What is also evident from the calculated structure of **11** is that the bidentate Lewis boron agent spatially protects the otherwise low-coordination chromium centre. This appears to retard the methylation of **7**, which, in its absence appears to proceed to **9**, stabilised as its AlMe$_3$ adduct **10**. The edge shift to higher energy in the absence of B(C$_6$F$_5$)$_3$ (Fig. 8) is consistent with the substitution at chromium of Cl by CH$_3$.
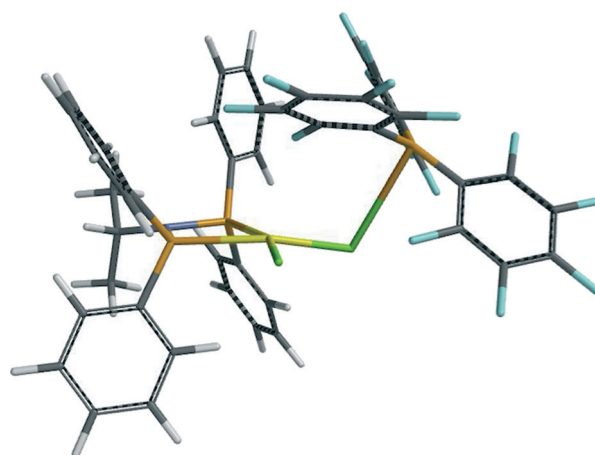
11a

(Yellow = Cr, light green = Cl, dark brown = B, brown = P, grey = C, purple = N, blue = F and white = H).
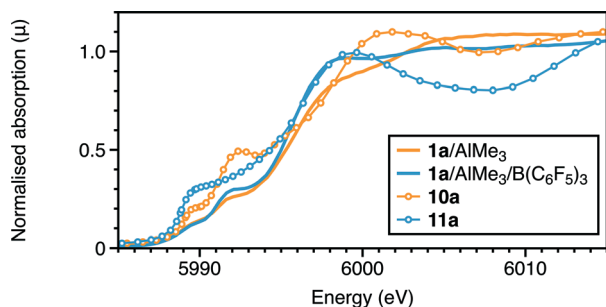
Fig. 8 Cr K-edge XANES: experimental and calculated spectra of **1a** with AlMe$_3$ with and without B(C$_6$F$_5$)$_3$.

3. Conclusions

These results provide strong evidence that, in the initial stages of the activation of the chromium tetramerisation catalyst, the (PPh$_2$)$_2$N(^{i}Pr) ligand allows rapid methylation of the chromium(III) centre. When comparing that to the homogeneous trimerisation chromium catalyst, [CrCl$_3${HN(CH$_2$CH$_2$S-decyl)$_2$}],[17] reaction with AlMe$_3$ proceeds to a chromium(II) stabilised intermediate [CrCl{N(CH$_2$CH$_2$S-decyl)$_2$}] in similar conditions after 1 second. A similar conversion to Cr(II), also driven by the formation of ethane by reductive elimination, takes several minutes with the aminophosphine ligand, and that complex probably exists as adducts with the Lewis acids AlMe$_3$ and B(C$_6$F$_5$)$_3$ (Scheme 1).

A previous XAFS study on the reaction of Cr(acac)$_3$, MMAO and (PPh$_2$)$_2$N(^{i}Pr) also proposed a Cr(II) product with a mean Cr–C coordination of 1.5 ± 0.6.[14] Bond distances similar to our EXAFS analysis at (Cr–C 2.03 Å, Cr–P at 2.42 Å), were

reported and also, there was no evidence in the EXAFS of Cr dimer formation. More closely related chemically is the study by Labinger and Bercaw using EPR and UV-visible spectroscopy to study the activation process by MAO with a bifunctional ligand bearing hemilabile donor groups *e.g.* [CrCl$_3$-{P(C$_6$H$_4$OMe)$_2$N(Me) P(C$_6$H$_4$OMe)$_2$}].[28] The initial product was reported as a trialkylated product, [Cr^{III}R$_3$(PNP)] and was accompanied with a much larger shift of the lowest energy band o the visible region than observed in this work where the alkylation has not proceeded so far.

The Lewis acid, [Ph$_3$C][Al{OC(^{t}Bu^F)$_3$}$_4$], accelerates the reduction to Cr(II), but under ambient conditions it causes the loss of the (PPh$_2$)N(^{i}Pr)PPh$_2$ ligand, with the metal sequestered in a dimer related to [Cr$_2$Me$_8$]$^{4-}$ in terms of structure around Cr (Scheme 1). Indeed, the reaction of [Ph$_3$C][Al{OC(^{t}Bu^F)$_3$}$_4$] with (PPh$_2$)N(^{i}Pr)PPh$_2$ has been previously reported.[20] The ligand is calculated to be relatively weakly bound to Cr(III), with complex formation of **1a** for *mer*-CrCl$_3$(THF)$_3$ only slightly exoergic (4.4 kcal mol^{-1}). Again this is in marked contrast to the coexistence of [CrCl{N(CH$_2$CH$_2$S-decyl)$_2$}] and [Ph$_3$C][Al{OC(^{t}Bu^F)$_3$}$_4$].[17] In contrast, the effect of B(C$_6$F$_5$)$_3$ may be to retard the alkylation at chromium(II).

However, under ethene oligomerisation reaction conditions with an excess of aluminoxanes,[5,29,30] or with this co-catalyst itself[31] ligands like (PPh$_2$)$_2$N(^{i}Pr) do alter the catalytic selectivity from a phosphine free system. Detailed calculations of the oligomerisation mechanism have been carried out using a smaller ligand system [Cr{PMe$_2$N(Me)PMe$_2$}], based upon Cr(I)–Cr(III) catalytic cycle.[32] As we observed for the [CrCl$_3${HN(CH$_2$CH$_2$S-decyl)$_2$}] system,[17] reduction to Cr(I) was not evident under our experimental conditions, although Cr(I) has been reported in a minor species using MAO as the aluminium reagent.[28] In the [CrCl$_3${HN(CH$_2$CH$_2$S-decyl)$_2$}] system,[17] DFT calculations did show much stronger binding of ethene to Cr(I) rather than Cr(II). This suggests that ethene could extend the chromium chemistry beyond that in Scheme 1, in order to favour sites more suited to phosphine coordination and promote this further reduction.

4. Experimental

Synthesis of [CrCl$_3${PPh$_2$N(R)PPh$_2$}(THF)] 1a (R = ^{i}Pr)

Ph$_2$N(^{i}Pr)PPh$_2$ (ref. 5) (0.20 g, 0.468 mmol) was added to a solution of [CrCl$_3$(THF)$_3$] (ref. 33) (0.175 g, 0.468 mmol) in dry/degassed CH$_2$Cl$_2$ (15 mL). The resulting mixture was stirred at room temperature under N$_2$ for 1 hour, and the solvent removed *in vacuo* to afford **1a** as a blue solid (0.194 g, 0.295 mmol, 63%). EA calc (found) %: C 56.49 (56.59), H 5.38 (5.36), N 2.09 (2.13). UV-vis (ε, M^{-1} cm^{-1}): 14 260 (300) and 19 910 (233) cm^{-1}. IR (cm^{-1}) includes 1060, 1012, 860 (THF) and 372, 345, 315 (Cr–Cl).

Cr K-edge XAFS measurements

These were performed on freshly prepared samples of **1a** were performed at the B18 beamline at Diamond Light Source in Didcot, England and BM26A (DUBBLE) of the
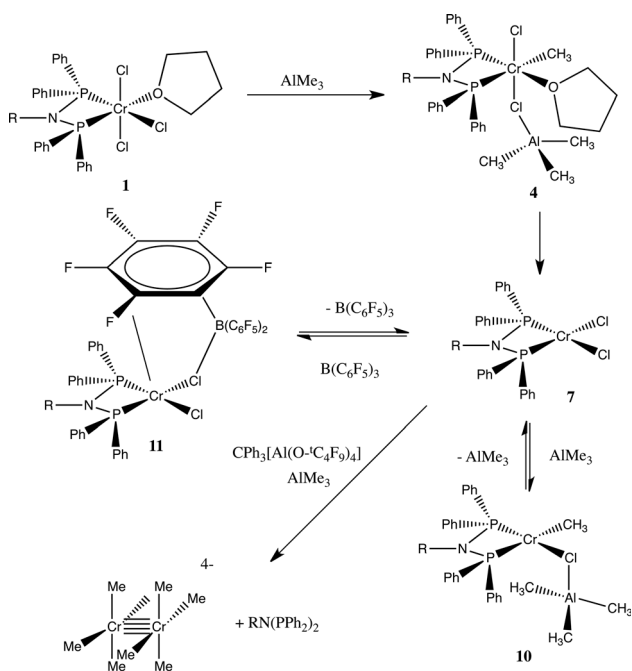
Scheme 1 Proposed reaction scheme from the interaction of **1a** with Al$_2$Me$_6$ and other Lewis acids. The formula [Cr$_2$Me$_8$]$^{4-}$ is only representative of the type of Cr site.

ESRF. Si(111) double crystal monochromators were used in combination with a Ge 9 element detector for fluorescence acquisition on all samples. Cr K-edge scans were obtained in 20 min. All spectra were calibrated using a Cr foil. XAS data processing and EXAFS analysis were performed using IFEFFIT[34] using the Hoare package.[35] All reactions were carried out at ambient temperature. Freeze quench experiments were performed on B18 by addition of $AlMe_3$ (with and without a Lewis acid) to $[CrCl_3\{PPh_2N(R)PPh_2\}(THF)]$ **1a** (R = ^iPr) (5 mM) in toluene solutions and then by transfer under argon to a Kapton tube with a liquid nitrogen. The samples were maintained frozen as previously described.[15]

Computational methods

The FEFF9 code was used to perform *ab initio* self-consistent field, real-space, full multiple scattering calculations.[36] The calculations were performed using the Hedin–Lundquist exchange correlation potential. A (final state rule) core hole is included on the absorber atom to mimic the final state of the photon absorption process. To allow a direct comparison of calculated and experimental XANES spectra, all calculated XANES underwent the same energy shift (eV) which was established using the experimental $[CrCl_3(PNP)(THF)]$ data as a reference, shifting the calculated fac-$[CrCl_3(PNP)(THF)]$ spectrum to the same energy as the experimental data, using the first derivative of the absorption edge.

Density functional theory calculations were performed using Spartan '14.[37] B3LYP and EDF2 functionals appeared to overestimate the stiffness of the bidentate ligand, which have a small chelate angle in the crystal (P–Cr–P 66.0°).[20] These methods also introduced a significant asymmetry to the Cr–P distances (0.08 Å), which was greatly reduced with the ωB97X-D method (0.05 Å). Some improvement was gained by adding the p-type polarisation functions on hydrogen atoms, and so candidate structures were investigated with EDF2 and also ωB97X-D functionals and 6-31G* and 6-31G** basis sets. The spin state for the Cr(III) was maintained as $S = 3/2$, consistent with the UV-visible spectra of **1a**. For Cr(II) species, $[CrXX'\{Ph_2N(Me)PPh_2\}]$ (X, X′ = Cl or Me), the $S = 1$ and $S = 0$ spin states were calculated to be ~25 and ~50 kcal mol^{-1} less stable than the high spin state ($S = 2$); hence all data presented here are for the $S = 2$ state.

Acknowledgements

Notes and references

1 Nexant Process Evaluation Research Planning (PERP), Report-Alpha Olefins 06/07-5, 2008.

2 D. Vogt, B. Cornils and W. A. Herrmann, *Oligomerization of Ethylene to Higher Linear α-Olefins: In Applied Homogeneous Catalysis with Organometallic Compounds*, VCH, New York, 1996, vol. 1, pp. 245–258.

3 D. S. McGuinness, *Chem. Rev.*, 2011, **111**, 2321–2341.

4 T. Agapie, *Coord. Chem. Rev.*, 2011, **255**, 861–880.

5 A. Bollmann, K. Blann, J. T. Dixon, F. M. Hess, E. Killian, H. Maumela, D. S. McGuinness, D. H. Morgan, A. Neveling, S. Otto, M. Overett, A. M. Z. Slawin, P. Wasserscheid and S. Kuhlmann, *J. Am. Chem. Soc.*, 2004, **126**, 14712–14713.

6 T. Agapie, S. J. Schofer, J. A. Labinger and J. E. Bercaw, *J. Am. Chem. Soc.*, 2004, **126**, 1304–1305.

7 A. K. Tomov, J. J. Chirinos, D. J. Jones, R. J. Long and V. C. Gibson, *J. Am. Chem. Soc.*, 2005, **127**, 10166–10167.

8 A. Jabri, P. Crewdson, S. Gambarotta, I. Korobkov and R. Duchateau, *Organometallics*, 2006, **25**, 715–718.

9 D. S. McGuinness, D. B. Brown, R. P. Tooze, F. M. Hess, J. T. Dixon and A. M. Z. Slawin, *Organometallics*, 2006, **25**, 3605–3610.

10 A. J. Rucklidge, D. S. McGuinness, R. P. Tooze, A. M. Z. Slawin, J. D. A. Pelletier, M. J. Hanton and P. B. Webb, *Organometallics*, 2007, **26**, 2782–2787.

11 I. Y. Skobelev, V. N. Panchenko, O. Y. Lyakin, K. P. Bryliakov, V. A. Zakharov and E. P. Talsi, *Organometallics*, 2010, **29**, 2943–2950.

12 L. McDyre, E. Carter, K. J. Cavell, D. M. Murphy, J. A. Platts, K. Sampford, B. D. Ward, W. F. Gabrielli, M. J. Hanton and D. M. Smith, *Organometallics*, 2011, **30**, 4505–4508.

13 S. Peitz, B. R. Aluri, N. Peulecke, B. H. Müller, A. Wöhl, W. Müller, M. H. Al-Hazmi, F. M. Mosa and U. Rosenthal, *Chem. – Eur. J.*, 2010, **16**, 7670–7676.

14 J. Rabeah, M. Bauer, W. Baumann, A. E. C. McConnell, W. F. Gabrielli, P. B. Webb, D. Selent and A. Brückner, *ACS Catal.*, 2013, **3**, 95–102.

15 S. A. Bartlett, P. P. Wells, M. Nachtegaal, A. J. Dent, G. Cibin, G. Reid, J. Evans and M. Tromp, *J. Catal.*, 2011, **284**, 247–258.

16 S. A. Bartlett, G. Cibin, A. J. Dent, J. Evans, M. J. Hanton, G. Reid, R. P. Tooze and M. Tromp, *Dalton Trans.*, 2013, **42**, 2213–2223.

17 S. A. Bartlett, J. Moulin, M. Tromp, G. Reid, A. J. Dent, G. Cibin, D. S. McGuinness and J. Evans, *ACS Catal.*, 2014, **4**, 4201–4204.

18 S. A. Bartlett, *PhD Thesis*, University of Southampton, 2012.

19 J. Moulin, *PhD Thesis*, University of Southampton, 2006.

20 D. S. McGuinness, M. Overett, R. P. Tooze, K. Blann, J. T. Dixon and A. M. Z. Slawin, *Organometallics*, 2007, **26**, 1108–1111.

21 S. Teo, Z. Weng and T. S. A. Hor, *Organometallics*, 2008, **27**, 4188–4192.

22 J. O. Moulin, J. Evans, D. S. McGuinness, G. Reid, A. J. Rucklidge, R. P. Tooze and M. Tromp, *Dalton Trans.*, 2008, 1177–1185.

23 R. A. Heintz, S. Leelasubcharoen, L. M. Liable-Sands, A. L. Reingold and K. H. Theopold, *Organometallics*, 1998, **17**, 5477–5485.

24 M. Tromp, J. Moulin, G. Reid and J. Evans, *AIP Conf. Proc.*, 2007, **882**, 699–701.

25 J. Krausse, G. Marx and G. Schödl, *J. Organomet. Chem.*, 1970, **21**, 159–168.

26 J.-D. Chai and M. Head-Gordon, *Phys. Chem. Chem. Phys.*, 2008, **10**, 6615–6620.

27 K. Yang, J. Zheng, Y. Zhao and D. G. Truhlar, *J. Chem. Phys.*, 2010, **132**, 164117.

28 L. H. Do, J. A. Labinger and J. E. Bercaw, *ACS Catal.*, 2013, **3**, 2582–2585.

29 M. J. Overett, K. Blann, A. Bollmann, J. T. Dixon, D. Haasbroek, E. Killian, H. Maumela, D. S. McGuinness and D. H. Morgan, *J. Am. Chem. Soc.*, 2005, **127**, 10723–10730.

30 Y. Shaikh, K. Albahily, M. Sutcliffe, V. Fomitcheva and S. Gambarotta, *Angew. Chem., Int. Ed.*, 2012, **51**, 1366–1369.

31 D. S. McGuinness, A. J. Rucklidge, R. P. Tooze and A. M. Z. Slawin, *Organometallics*, 2007, **26**, 2561–2569.

32 D. S. McGuinness, B. Chan, G. J. P. Britovsek and B. F. Yates, *Aust. J. Chem.*, 2014, **67**, 1481–1490.

33 R. J. Kern, *J. Inorg. Nucl. Chem.*, 1962, **24**, 1105–1109.

34 M. J. Newville, *J. Synchrotron Radiat.*, 2001, **8**, 322–324.

35 B. Ravel and M. J. Newville, *J. Synchrotron. Radiat.*, 2005, **12**, 537–541.

36 J. J. Rehr, J. J. Kas, M. P. Prange, A. P. Sorini, Y. Takimoto and F. Vila, *C. R. Phys.*, 2009, **10**, 548–559; J. J. Rehr, J. J. Kas, F. D. Vila, M. P. Prange and K. Jorissen, *Phys. Chem. Chem. Phys.*, 2010, **12**, 5503–5513.

37 *Spartan '14*, Wavefunction Inc., Irvine, CA10; Y. Shao, L. F. Molnar, Y. Jung, J. Kussmann, C. Ochsenfeld, S. T. Brown, A. T. B. Gilbert, L. V. Slipchenko, S. V. Levchenko, D. P. O'Neill, R. A. DiStasio Jr, R. C. Lochan, T. Wang, G. J. O. Beran, N. A. Besley, J. M. Herbert, C. Y. Lin, T. Van Voorhis, S. H. Chien, A. Sodt, R. P. Steele, V. A. Rassolov, P. E. Maslen, P. P. Korambath, R. D. Adamson, B. Austin, J. Baker, E. F. C. Byrd, H. Dachsel, R. J. Doerksen, A. Dreuw, B. D. Dunietz, A. D. Dutoi, T. R. Furlani, S. R. Gwaltney, A. Heyden, S. Hirata, C. P. Hsu, G. Kedziora, R. Z. Khalliulin, P. Klunzinger, A. M. Lee, M. S. Lee, W.-Z. Liang, I. Lotan, N. Nair, B. Peters, E. I. Proynov, P. A. Pieniazek, Y. M. Rhee, J. Ritchie, E. Rosta, C. D. Sherrill, A. C. Simmonett, J. E. Subotnik, H. L. Woodcock III, W. Zhang, A. T. Bell, A. K. Chakraborty, D. M. Chipman, F. J. Keil, A. Warshel, W. J. Hehre, H. F. Schaefer III, J. Kong, A. I. Krylov, P. W. Gill and M. Head-Gordon, *Phys. Chem. Chem. Phys.*, 2006, **8**, 3172–3191.